Journal of Stress Analysis
Vol. 6, No. 1, Spring – Summer 2021, 127-138
Bu-Ali Sina University

ORIGINAL RESEARCH PAPER

An Investigation into the Effect of Strain Rate on Damage Evolution in Pure Copper Using a Modified Bonora Model

G.H. Majzoobi*, S.S. Jafari
Mechanical Engineering Department, Bu-Ali Sina University, Hamedan, Iran.

Article info

Article history:
Received 12 July 2021
Received in revised form
11 September 2021
Accepted 13 September 2021

Keywords:
Strain rate
Ductile damage
Bonora damage model
Numerical simulation

Abstract

Strain rate is an effective parameter in characterization of ductile materials. In this work, the influence of strain rate on damage evolution in copper is investigated through analytical approach, experiment, and numerical simulation. In the analytical approach, a modified damage model is proposed to take account of the effect of strain rate on damage parameter based on Continuum Damage Mechanics (CDM). A new technique is used for evaluation of damage evolution in tensile dog bone specimens using a Split Hopkinson Tensile Bar (SHTB). The results of high strain rate tests are used to validate the modified damage model. The proposed model is based on Bonora ductile damage model in which the effect of strain rate is incorporated. The numerical simulations are performed by implementing the proposed model in the finite element commercial code, ABAQUS/Explicit using VUSDFLD subroutines. A reasonable agreement was observed between the experimental data and the proposed damage model.

1. Introduction

The damage evolution in ductile materials has been the subject of many investigations over the past few decades. From micromechanical and meso-scale point of view, the damage in ductile materials is caused by void nucleation, growth, and coalescence [1]. The micro-mechanical theories (Gourson-Tvergaard-Needleman (GTN) [2, 3] and Rousselier [4, 5]) and Continuum Damage Mechanics ((CDM) Lemaitre [6], Voyiadjis [7] and Bonora [8]) are the two well-known methods which are widely used for the study of damage evolution in metals.

Most researchers employ CDM to investigate the damage evolution in particular for ductile metals [6-10]. The reduction of Young's modulus in loading-unloading tests (stiffness degradation test) is one of the well-known methods to evaluate the damage evolution [8, 11]. According to the method, the damage evolution (D) is defined as $D = 1 - (E/E_0)$, where E_0 and E are the initial and current Young's modulus, respectively. Damage parameter varies between zero and one; $0 \leq D \leq 1$ [6].

Bonora [8] proposed a new nonlinear damage model to predict the ductile fracture based on CDM. In the Bonora damage model (please see section 4 for the details), a nonlinear function is suggested which contains five damage parameters (threshold strain, fracture strain, initial damage, critical damage, and damage exponent). Bonora et al. [12] studied the effect of stress triaxiality on the ductile damage of Swedish and ARMCO iron by notched and plain specimens. They proposed a new model to predict spall fracture in a plate-impact test.

*Corresponding author: G.H. Majzoobi (Professor)
E-mail address: gh_majzoobi@yahoo.co.uk
http://dx.doi.org/10.22084/jrstan.2021.24907.1193
ISSN: 2588-2597

Bonora et al. [13] defined a new damage dissipation function to make the Bonora damage model to be applicable for shear-controlled damage as well. Pei et al. [14] combined mechanical behavior and fatigue performance through micro-structural investigation to study damage evolution of IN718 alloy under monotonic and cyclic loading conditions. They also investigated the forging effect on the damage evolution. They proposed the phenomenological damage model based on Bonora's model by determining loading-amplitude related parameter.

Guo et al. [15] applied a damage coupled elastic-plastic constitutive model considering multi-linear hardening relation to predict the behavior of turbine blade for Low Cycle Fatigue (LCF) conditions. They employed Runge-Kutta (RK) method for solving the process of damage accumulation. Yadollahi et al. [16] used a micro-mechanical damage model to determine the tensile damage evolution of Additive Manufactured (AM) 316L stainless steel. They defined micro-structural features (e.g. porosity) as internal state variables to predict the monotonic stress-strain behavior.

Kumar and Dixit [17] investigated the damage of steel (IS 2062: 2006GR E410W A) and proposed a new damage model with few parameters. However, the identification of the constants of their model was more complex than the other models such as Bonora [8], Chandrakanth and Pandey [18] and Thakkar and Pandey [19] models.

The strain rate is an important parameter in materials behavior particularly in metal forming processes such as stamping, hydroforming, explosive forming, electro hydro forming and powder compaction etc [20-24]. Split Hopkinson Pressure Bar (SHPB) or Split Hopkinson Tensile Bar (SHTB) is the most well-known device to investigate the effects of strain rate on dynamic behavior of material.

Bonora et al. [25] used hourglass-shaped rectangular tensile specimen to study the behavior of SA537 C11 Steel at low strain rates. They found that in low deformation rates, variation of strain rate has no effect on damage measurement.

Sari Sarraf et al. [26] employed an X-ray tomography analysis and predicted the damage evolution based on Rousselier damage model considering different hardening models (modified Johnson-Cook [27], Voce-modified Johnson-Cook [28, 29] and Khan and Liang [30]) at different strain rates ranging from 0.001 to 100 s^{-1}. Husson et al. [31] proposed a nonlinear damage model by considering strain rate, temperature and micro-structure effects. Their model depends on fracture strain and critical damage, while it is not sensitive to threshold strain.

Jafari et al. [32] developed a new technique to investigate the strain rate effects on ductile damage evolution. They determined the damage evolution based on material stiffness reduction. They showed that the strain rate has considerable effects on the damage evolution, but the way the strain rate affects the damage evolution is not known well enough.

The main objective of this study is to modify the Bonora damage model to take account of the effects of high strain rate on damage evolution of the pure copper. A new experimental technique [32] is employed to measure the damage evolution in high strain rate and quasi-static tensile tests. From the experimental variation of damage parameter versus the equivalent plastic strain obtained at different strain rates, the effects of strain rate is evaluated and is incorporated into the Bonora damage model. The modified Bonora model is implemented in a user material subroutine, VUSDFLD, in the finite element code ABAQUS/Explicit. The model is validated by using the experimental results.

2. Material and Test Device

In order to evaluate the effect of high strain rate on damage evolution, the specimen used by Jafari et al. [32] was employed for tensile dynamic tests accomplished using a split Hopkinson bar. The specimen comprises two segments: real and dummy. The specimen assembly and real view shown in Fig. 1 consist of a specimen and a locker marked by 1 and 4, respectively. The specimen itself consists of a dummy segment and a real segment indicated by 2 and 3, respectively. At the impact, the dummy segment is broken to release the impact energy to prevent any damage to the SHPB testing device in dynamic tests. The locker is used to adjust the amount of elongation that the real segment of specimen is designed to undergo. By controlling the specimen's elongation, the damage evolution can be controlled under dynamic loading conditions. After the specimen is elongated to the desired level, the real part of specimen is subjected to a conventional uniaxial tensile test under quasi-static loading condition (for more details refer to [32]) and the damage evolution is determined using material stiffness degradation test.

As stated before, damage is caused by void growth in a ductile material. In low ductile materials, damage evolution is hard to be detected and be measured by conventional tests such as cyclic tests. Therefore, a material with high ductility, pure copper, was employed in this study. In order to increase its ductility, the copper was annealed at 600°C for 2h and cooled in a furnace at a cooling rate of 25°C/h. The chemical compositions of the pure copper obtained using (X-ray fluorescence) XRF at room temperature are given in Table 1.

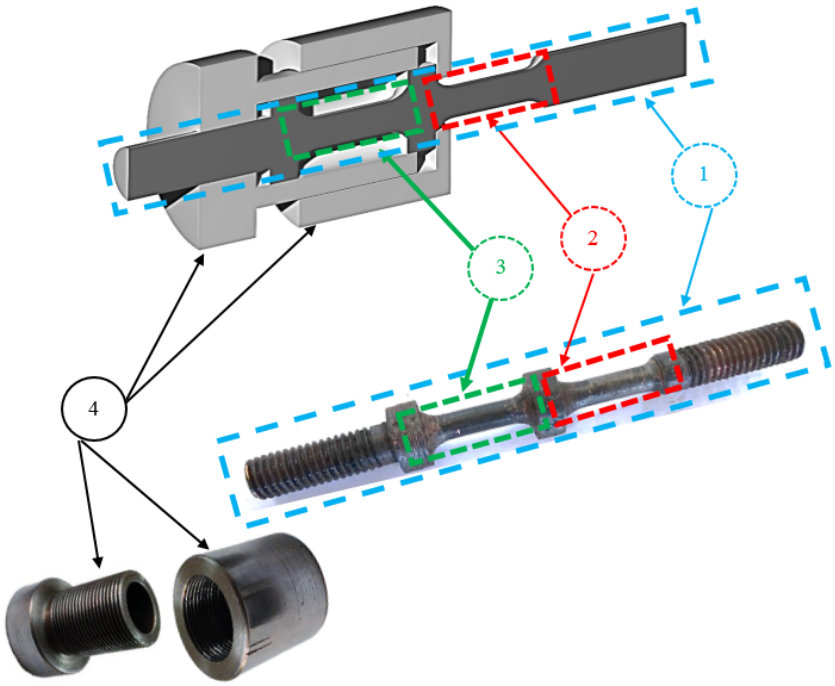

Fig. 1. Isometric and real view of the specimen including the real and dummy segments.

Table 1
Chemical composition of pure copper

Element	Cu	Co	Fe	Pb	Ni	Zn	Sn	P	Al	Impurities total
Quantity (%)	base	0.03	0.02	0.02	0.02	0.01	0.01	0.003	0.002	0.02

The schematic and the general view of the SHPB is depicted in Fig. 2. As the figure indicates, the two strain gauges mounted at the middle of the incident and transmission bars are used to measure the stress waves travelling in the bars as the result of collision of the striker and the incident bars. From the strain gauges outputs, the stress-strain curve of the material can be obtained. More details can be found in [33].

As mentioned before, the specimen is subjected to two tests: SHTB and SANTAM. In the first test, the specimen is subjected to tensile loading using SHTB in a way that the real segment of the specimen undergoes a specific Plastic deformation without being fractured and the dummy part of the specimen fails to release the energy of the impact. In the second test, the already deformed real part of the specimen is subjected to quasi-static tensile testing to measure the elasticity modulus for damage analysis. Typical specimens before and after test are shown in Figs. 1 and 3, respectively.

3. Material Model

Material model is an important requirement in any numerical simulation of damage using a commercial software. There are a variety of material models available in the literature. Ignoring the effect of temperature, typical models, which consider strain rate and are highly popular in simulation of materials deformation, are: (i) Johnson-cook (JC) model [34], (ii) the modified JC (mJC) model [35], (iii) Khan-Huang-Liang (KHL) model [30]. JC model is used in the current study to define the material model of the pure copper as follows:

$$\sigma = (C_1 + C_2\varepsilon_p^{C_3})\left[1 + C_4 \ln\left(\frac{\dot{\varepsilon}_p}{\dot{\varepsilon}_0}\right)\right] \qquad (1)$$

where $C_{1,\cdots,4}$ are the material's constants and ε_p, $\dot{\varepsilon}_p$, $\dot{\varepsilon}_0$ denote the equivalent plastic strain, the equivalent plastic strain rate, and the reference strain rate. Fig. 4 shows stress-strain curve of the pure copper at the strain rate of $630s^{-1}$.The constants of the material are identified from the true stress-strain curve using a curve fitting technique (SOLVER of the Microsoft Excel software is used as an iterative nonlinear optimization algorithm [36]). The (Rsq) of the fitting is 0.92 which is acceptable. The results are given in Table 2.

4. Ductile Damage Models

4.1. Bonora's Damage Model

As stated above, Bonora damage model was modified to take account of strain rate effects. In Bonora ductile damage model [8] the effective stress (σ_{eff}) is defined as follows:

$$\sigma_{eff} = \frac{\sigma}{1 - D} \qquad (2)$$

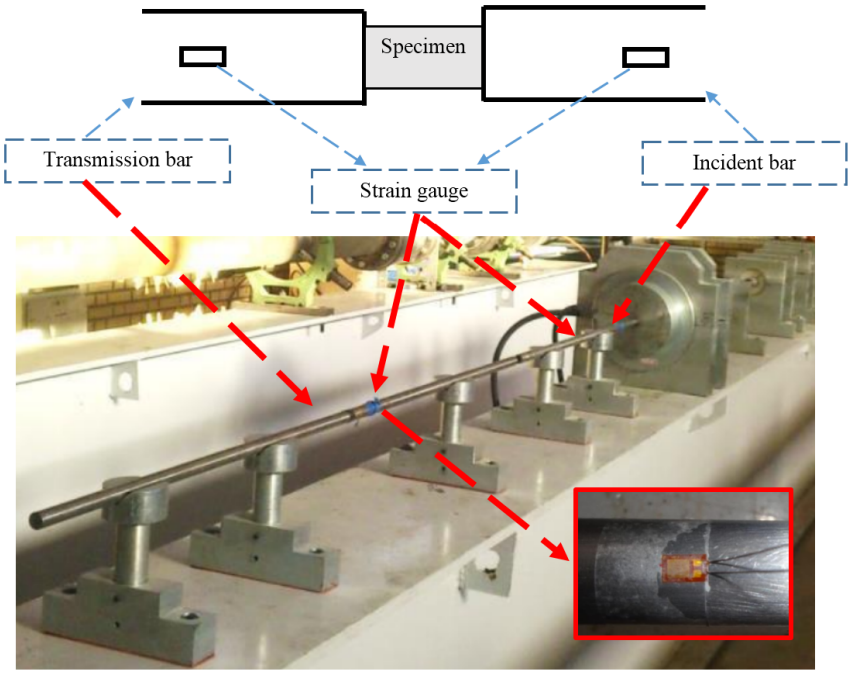

Fig. 2. Schematic and real view of incident and transmission bars of SHPB.

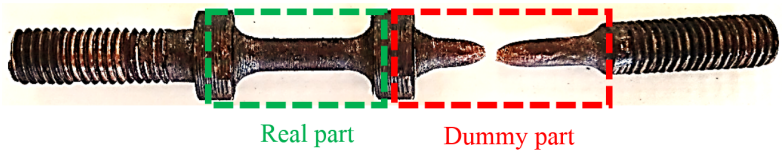

Fig. 3. Typical specimen after high rate test.

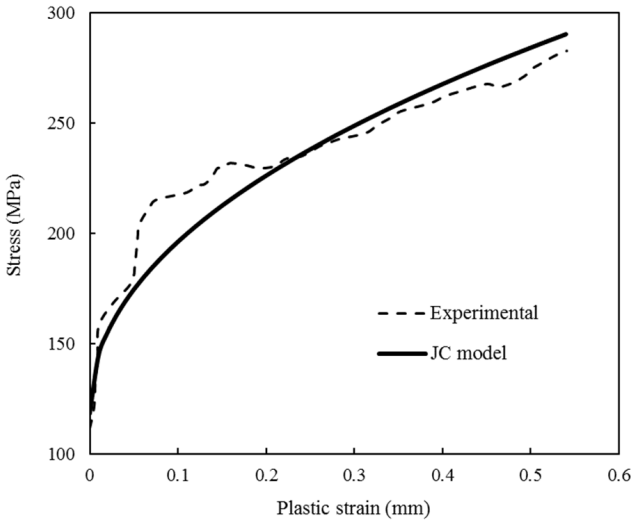

Fig. 4. A comparison between the experimental stress-strain curves obtained by experiment (dashed lines) and predicted by Johnson-cook model (solid lines) at $\dot{\varepsilon} = 630\text{s}^{-1}$.

Table 2
The constants of JC model.

C_1	C_2	C_3	C_4
104.7	203.4	0.47	0.046

where, σ and D are stress and damage parameters, respectively. Damage parameter is defined as follows:

$$D = \frac{E_0 - E}{E_0} \tag{3}$$

In which E_0 and E are the initial and the current Young's modulus, respectively. Bonora [8] considered the strain equivalence hypothesis to develop his model and suggested a damage potential function (F_D) as:

$$F_D = \left[\frac{1}{2}\left(-\frac{Y}{S_0}\right)^2 \frac{S_0}{1-D}\right] \frac{(D_{cr}-D)^{(\frac{\alpha-1}{\alpha})}}{p^{(\frac{2+n}{n})}} \tag{4}$$

where Y, S_0, D_{cr}, p, α and n are the damage energy release rate, material constant, critical damage, effective equivalent accumulated plastic strain, the damage exponent, and the material hardening exponent, respectively. For the uniaxial loading case and after using the specified function and some mathematical simplification, the damage variable is obtained as follows:

$$D = D_{cr}\left\{1 - \left[1 - \frac{\ln\left(\frac{\varepsilon_p}{\varepsilon_{th}}\right)}{\ln\left(\frac{\varepsilon_{cr}}{\varepsilon_{th}}\right)}\right]^{\alpha}\right\} \tag{5}$$

where ε_p, ε_{cr} and ε_{th} are plastic strain, critical strain and threshold strain, respectively. In Bonora damage

model, four constants (D_{cr}, α, ε_{th}, and ε_{cr}) are obtained from the variation of damage parameter versus plastic strain curve using a curve fitting technique.

Determination of Young's modulus from loading-unloading test, is accompanied by some errors due to clip gauge slip. Bonora et al. [37] used finite element simulation and corrected the current Young's modulus for ductile metals by suggesting a calibration function depending on the engineering strain as follows:

$$\tilde{E} = K^{\exp}(\Delta l)\frac{l_0}{A_0}\frac{1}{f(\Delta l)} \tag{6}$$

where $K^{\exp}(\Delta l)$, l_0, A_0, and $f(\Delta l)$ are the slop of experimental force-displacement curve, reference gauge, reference area, and calibration function, respectively. The calibration function is defined as:

$$f(\Delta l) = \frac{1}{(1+\varepsilon_{eng})^2} \tag{7}$$

where ε_{eng} is the strain at the point where the extrapolation of each unloading straight line intercepts the horizontal coordinate axis for each unloading line (see Fig. 5). Typical stress-strain curve obtained from a loading-unloading test for pure copper is shown in Fig. 5.

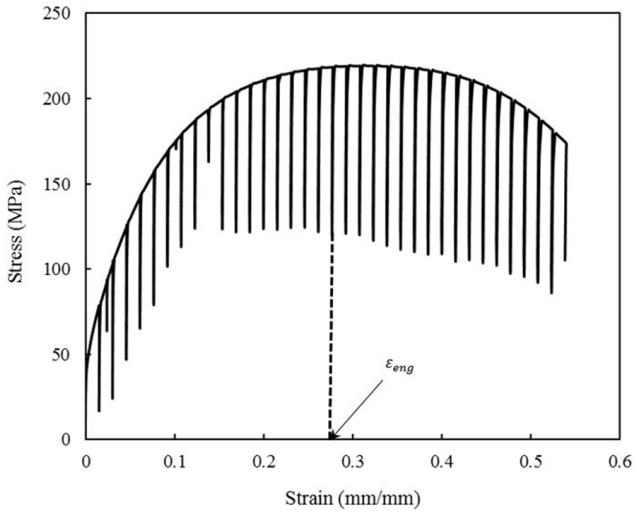

Fig. 5. A cyclic loading-unloading tensile test for pure copper.

By measuring the Young's modulus in each cycle of loading-unloading curve variation of Young's modulus versus plastic strain was obtained. The results for quasi-static test are shown in Fig. 6. Variation of damage parameter versus plastic strain was then obtained using Eq. (5). The results are illustrated in Fig. 7. As the figures suggest, by increasing plastic strain, Young's modulus decreases, while damage increases with the increase of plastic strain. From Fig. 6 and using a curve fitting technique, the constants of the Bonora damage model defined by Eq. (5) were obtained. The results for pure copper are given in Table 3.

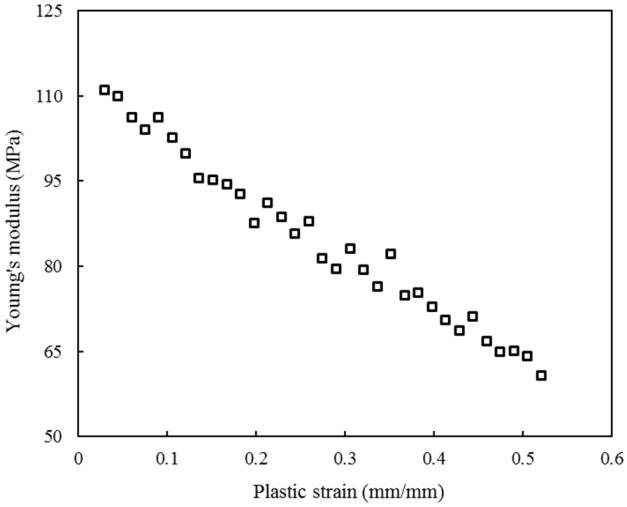

Fig. 6. Variation of Young's modulus vs plastic strain.

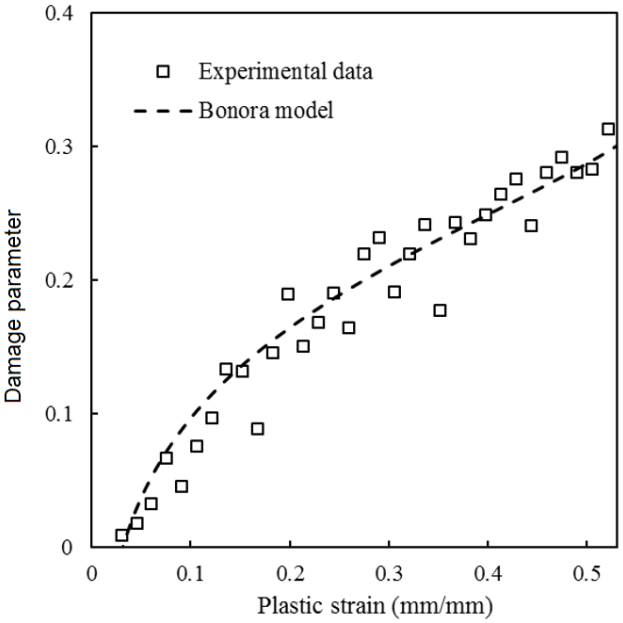

Fig. 7. Damage parameter vs plastic strain in quasi-static test for pure copper.

Table 3
The constants of Bonora damage model for quasi-static loading.

D_{cr}	ε_{th}	ε_f	α
0.32	0.0318	0.56	0.7

As mentioned before, the effect of strain rate was ignored in Bonora damage model. In order to assess the accuracy of the Bonora model, damage parameter was calculated using Eq. (5) (Bonora model). A comparison between the damage parameter obtained by experiment for 4 different strain rates of quasi-static, 630, 1115, and 1700s^{-1} and predicted by Bonora model is shown in Fig. 8. As the figure suggests, damage parameter varies with strain rate. The error in the damage parameter for different strain rates and due to

neglecting the effect of strain rate in Bonora model is presented in Fig. 9. As the figure implies, the damage parameter predicted by Bonora damage model agrees reasonably well with the experimental results for quasi-static loading. However, the accuracy of the model diminishes significantly as the strain rate increases, so that for the strain rate of $1700s^{-1}$, this discrepancy amounts to 50% which cannot be ignored.

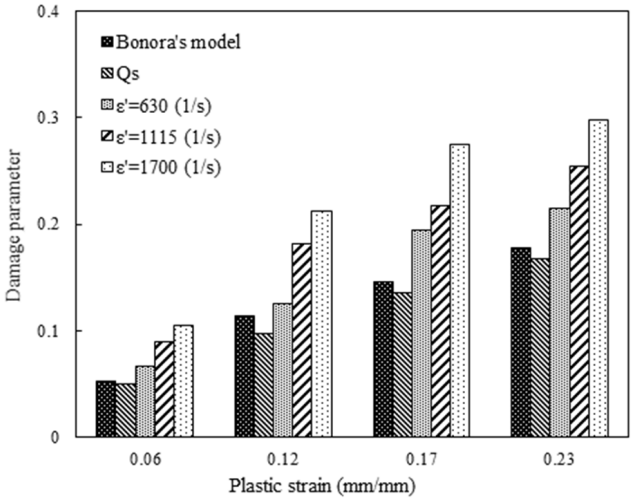

Fig. 8. A comparison between the damage parameter obtained by experiment for different strain rates and predicted by Bonora damage model.

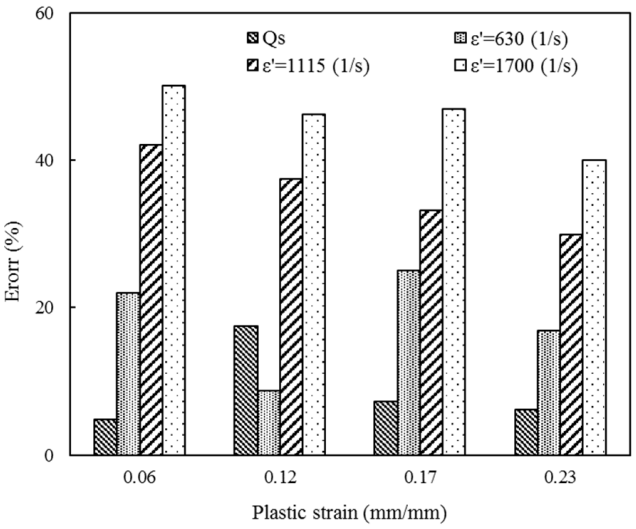

Fig. 9. The error in damage parameter for different strain rates due to neglecting the effect of strain rate in Bonora model.

4.2. Modification of Bonora Damage Model

As stated before, most of the damage models such as the one defined by Eq. (5) (Bonora damage model) ignore the effect of strain rate. In this section the effect of strain rate on damage evolution is investigated by examining the strain rate dependency of the constants of the Bonora's damage model defined by Eq. (5). Variation of damage evolution versus plastic strain for different strain rates is shown in Fig. 10. By using a curve fitting technique, the constants of Bonora's damage model can be determined from Fig. 9. Due to the physical definition of threshold strain (ε_{th}) [8], this parameter is not sensitive to strain rate and is constant, $\varepsilon_{th} = 0.0318$. Moreover, the fracture strain (ε_f) can be measured from the stress-strain curve obtained from SHPB test for different strain rates. The two remaining constants (critical damage and damage exponent) are computed from the curve fitting of damage parameter-plastic strain diagram for different strain rates. The results are provided in Table 4. As the table indicates, the critical damage and damage exponent are significantly sensitive to strain rate. Now, this rate dependency can be cast into an empirical relation leading to modification of Bonora model. In fact, the modified Bonora damage model is defined by Eq. (5) except that its two constants, critical damage and damage exponent, are strain rate dependent.

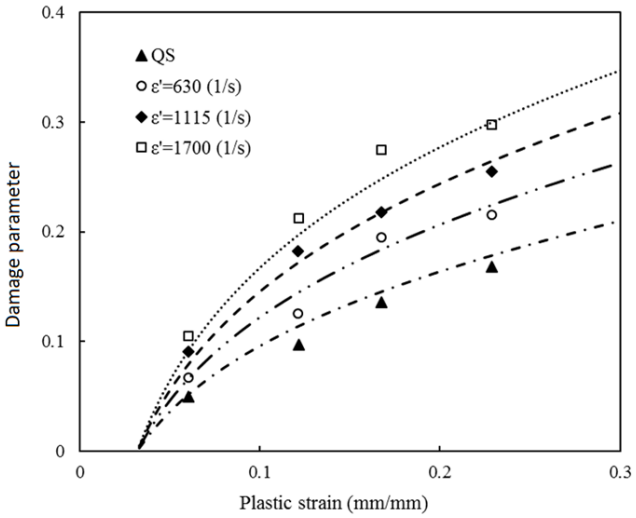

Fig. 10. Variation of damage parameter versus plastic strain obtained from experiment and predicted by the Bonora damage model for different strain rates.

Table 4
Fracture strain, critical damage and damage exponent at different strain rates.

$\dot{\varepsilon}$ (s^{-1})	ε_f	D_{cr}	α
Quasi-Static	0.56	0.32	0.70
630	0.54	0.38	0.75
1115	0.51	0.42	0.80
1700	0.48	0.46	0.85

Variation of critical damage, D_{cr}, and the damage exponent, α, versus the logarithmic dimensionless strain rate is depicted in Fig. 11. As the figure indicates, by increasing the logarithmic dimensionless strain rate, the critical and damage exponent increase. As the figure suggests, a linear trend governs the relation between the two constants and the logarithmic

dimensionless strain rate. The relation can be defined as follows for the two constants:

$$D_{cr}^{\mathrm{dyn}} = D_{cr}^{QS}\left(a_1 \log\left(\frac{\dot{\varepsilon}}{\dot{\varepsilon}_0}\right) + a_2\right) \tag{8}$$

$$\alpha^{\mathrm{dyn}} = \alpha^{QS}\left(b_1 \log\left(\frac{\dot{\varepsilon}}{\dot{\varepsilon}_0}\right) + b_2\right) \tag{9}$$

where $\dot{\varepsilon}$ and $\dot{\varepsilon}_0$ are the strain rate and reference strain rate, respectively. Furthermore, a_1, a_2, b_1, and b_2 are material constants which can be obtained from Fig. 11. The results are given in Table 5.

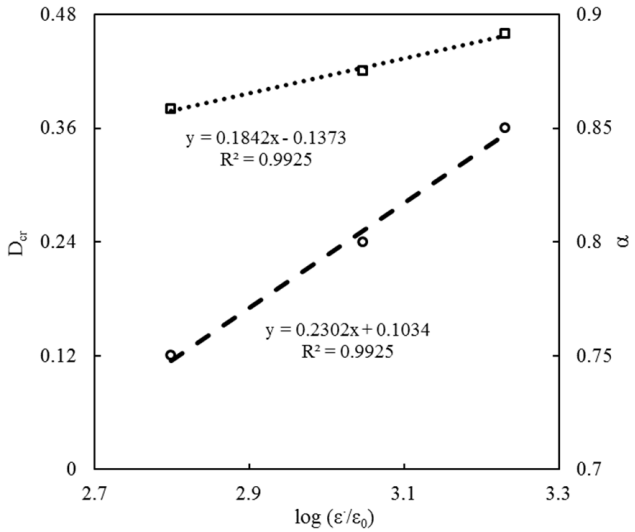

Fig. 11. Variations of damage exponent and critical damage parameter vs logarithmic dimensionless strain rate for pure copper.

Table 5
The values of material constants of Eqs. (8) and (9) for pure copper.

a_1	a_2	b_1	b_2
0. 576	-0.429	0.329	0.148

Eventually, by substituting Eqs. (8) and (9) in Bonora's damage model the modified Bonora damage parameter (D_{dyn}) can be defined as follows:

$$D_{dyn} = D_{cr}^{dyn}\left\{1 - \left[1 - \frac{\ln\left(\frac{\varepsilon}{\varepsilon_{th}}\right)}{\ln\left(\frac{\varepsilon_f^{dyn}}{\varepsilon_{th}}\right)}\right]^{\alpha_{dyn}}\right\} \tag{10}$$

where D_{cr}^{dyn} and α^{dyn} are critical damage and damage exponent in dynamic loading defined by Eqs. (9) and (10). In addition, ε_f^{dyn} is the dynamic fracture strain measured from stress-strain curves obtained from the SPHB tensile tests. A comparison between the damage parameters predicted by the modified Bonora's damage model and obtained from experiment for different strain rates is shown in Fig. 12.

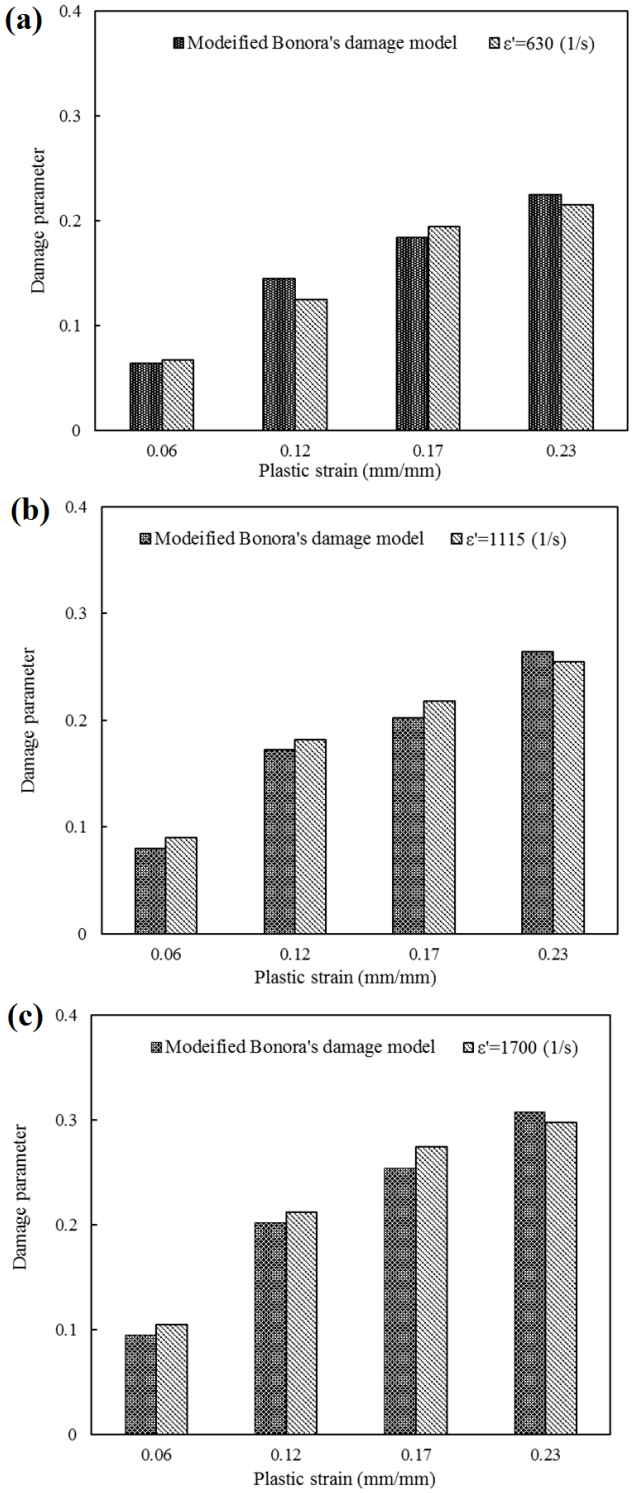

Fig. 12. Comparison between the damage parameters predicted by the modified Bonora's damage model and obtained from experiment for different strain rate, a) 630s^{-1}, b) 1115 s^{-1}, and c) 1700s^{-1}.

The error in damage parameter predicted by the modified Bonora model for different strain rates is shown in Fig. 13. As the figure demonstrates, the level of error of damage parameter predicted by the modified Bonora damage model (considering the effect of

strain rate) has decreased significantly compared with that predicted by the original Bonora model (ignoring the effect of strain rate) and shown in Fig. 9. It can easily be worked out from Fig. 9 and 13 that the mean error (for the three strain rates) has decreased from 30% for the original Bonora model to around 7% for the modified Bonora model. This discrepancy shows that the effect of strain rate on damage evolution in ductile materials such as the pure copper used in this work is quite considerable and cannot be ignored.

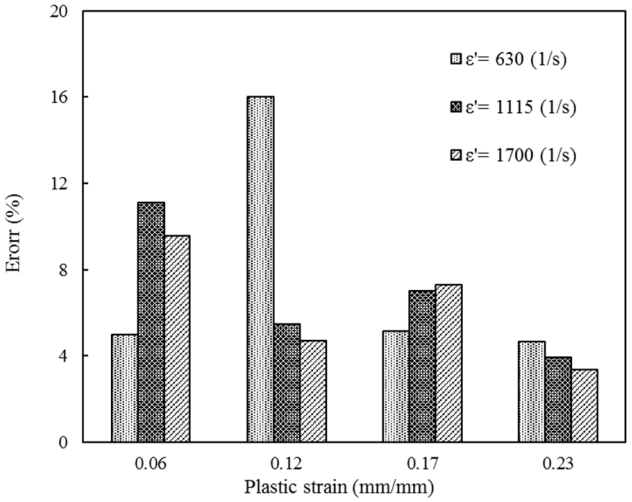

Fig. 13. The error in damage parameter predicted by the modified Bonora model for different strain rates.

The accuracy of Eqs. (8) and (9) was examined by conducting two new tests at the strain rates of 910, and 1450 s^{-1}. The results of the two new tests are compared with the results of the tests used for determining the constants of Eqs. (8) and (9) in Fig. 14. As the figure indicates, there is a reasonable agreement between the critical damage and damage component predicted by the equations and obtained by the experiment suggesting that Eqs. (8) and (9) are valid for the range of strain rate considered in this work.

The validity of the modified model, Eq. (10), was examined by making a comparison between the damage parameter obtained by experiment and predicted by the modified Bonora damage model for the strain rates which have not been used for determining the constants. The results are illustrated in Fig. 15. The constants used in the model, Eq. (10), were the same as those given in Table 5 for Eqs. (8) and (9). Again, a reasonable agreement between the experiments and the modified Bonora damage model is seen in the figure.

5. Numerical Implementation

In order to validate the proposed model (Eq. (10)), it was implemented in ABAQUS finite element software using a user subroutine called VUSDFLD.

The finite element model used in the simulations and the dimensions of the specimen are depicted in Fig. 16, where axisymmetric analysis is considered for the simulations. As it is seen, the model is quite similar to the specimen-locker assembly illustrated in Fig. 1. In addition, the finite strain and large deformation with Lagrangian update assumptions are considered in the simulations. Two steps adaptive re-meshing throughout of the gauge length is also employed to increase the accuracy of results during high rate deformation. The specimen's model comprises 664 elements and 801 nodes adopted after mesh convergence analysis. Moreover, the locker was assumed rigid to suppress any deformation other than that in the specimen. The boundary conditions were defined as they appeared in the experiments. In the simulation, the left hand side of specimen (transmit bar) was fixed and the velocity was applied on the right hand side of specimen (incident bar).

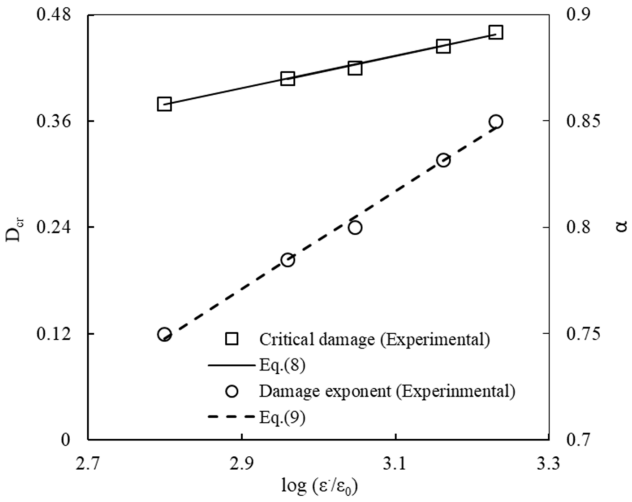

Fig. 14. A comparison between the critical damage obtained from experiments (symbols) and predicted by Eqs. (8) and (9) (lines) for different strain rates.

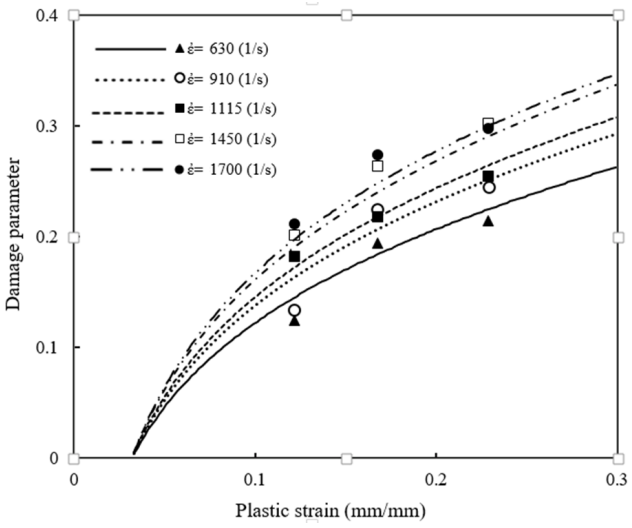

Fig. 15. Comparison between experiments data (symbols) and modification Bonora model (lines) for different strain rates.

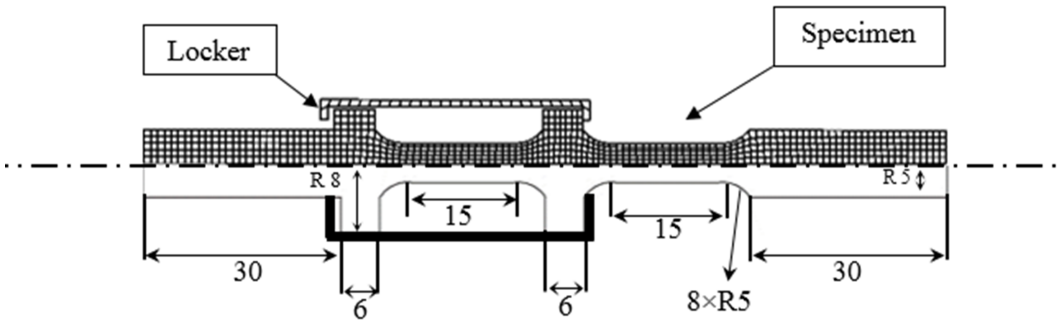

Fig. 16. F.E model of the specimen (all dimension in mm).

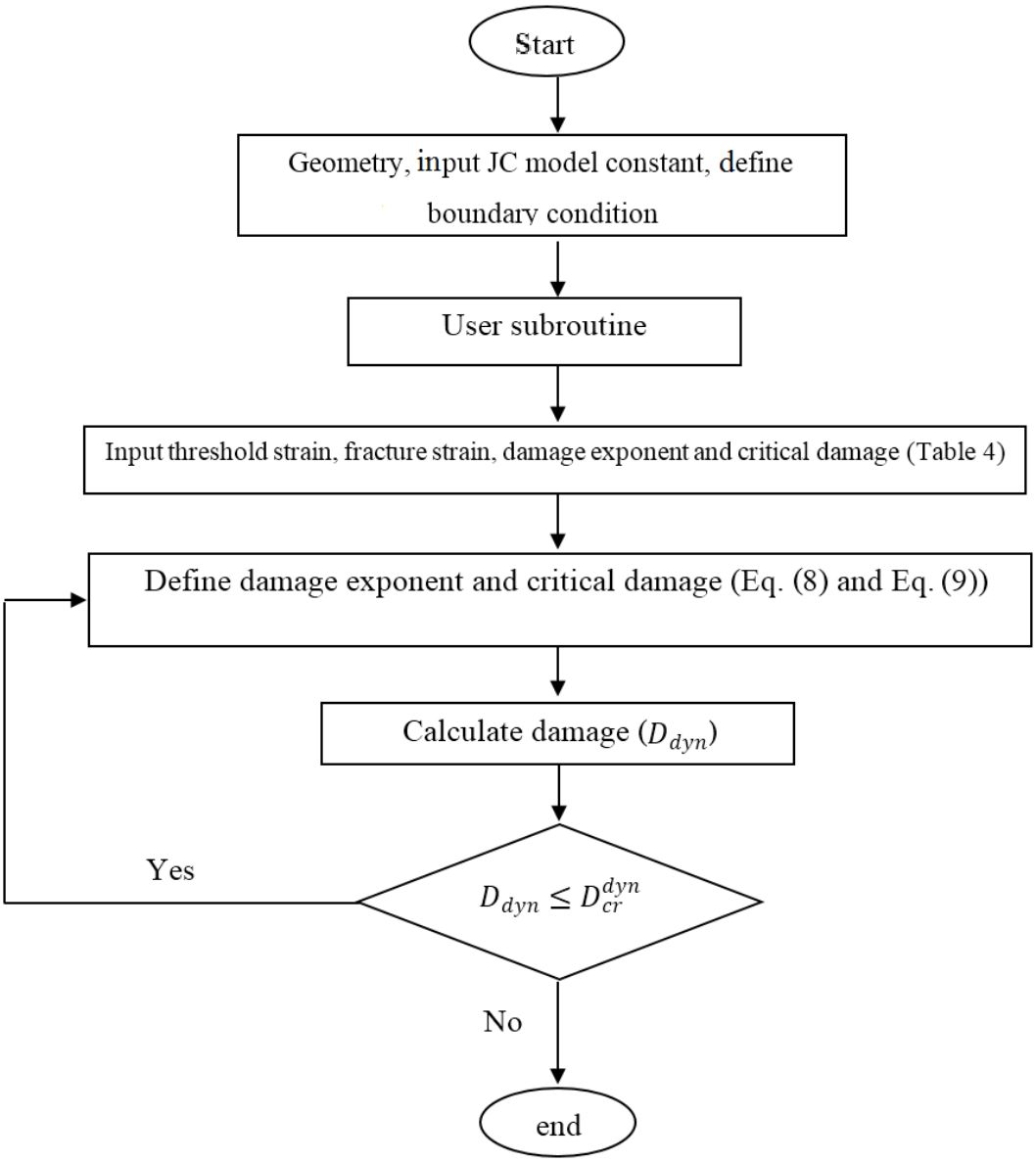

Fig. 17. Flowchart of the simulation and VUSDFLD subroutine.

It is obvious that the center line must be fixed in y direction because of axisymmetric simulation. The numerical solution strongly depends on the finite element mesh used in the analysis. In the numerical study, the number of elements was increased step by step from 330 to 664 element after which no change was observed in the results. Therefore, a mesh comprising 664 elements was considered in the finite element model of the

specimen in the simulations. The flowchart of the simulation and VUSDFLD subroutine operation is shown in Fig. 17.

As stated before, Bonora damage model was modified to take account of strain rate effects on material damage evolution. This was accomplished by establishing the relations between the damage parameters of Bonora model and strain rate. The strain rate dependent damage parameters were then implemented into a Fortran based user subroutine. Fig. 18 shows the damage contours at three strain rates of $630s^{-1}$, $1115s^{-1}$, and $1700s^{-1}$. As the figure suggests, the damage parameter increases with strain rate.

The critical damage obtained from the modified Bonora model and predicted by numerical simulation are given in Table 6. Additionally, the damage parameter for different plastic stain and strain rate are provided in Table 7. As the Table suggests, a reasonable agreement between the numerical simulations and the modified Bonora damage model is seen in the table.

Table 6
Critical damage for different strain rates.

Strain rate (1/s)	Critical damage	
	Modified model	VUSDFLD
630	0.360	0.372
1115	0.420	0.417
1700	0.460	0.458

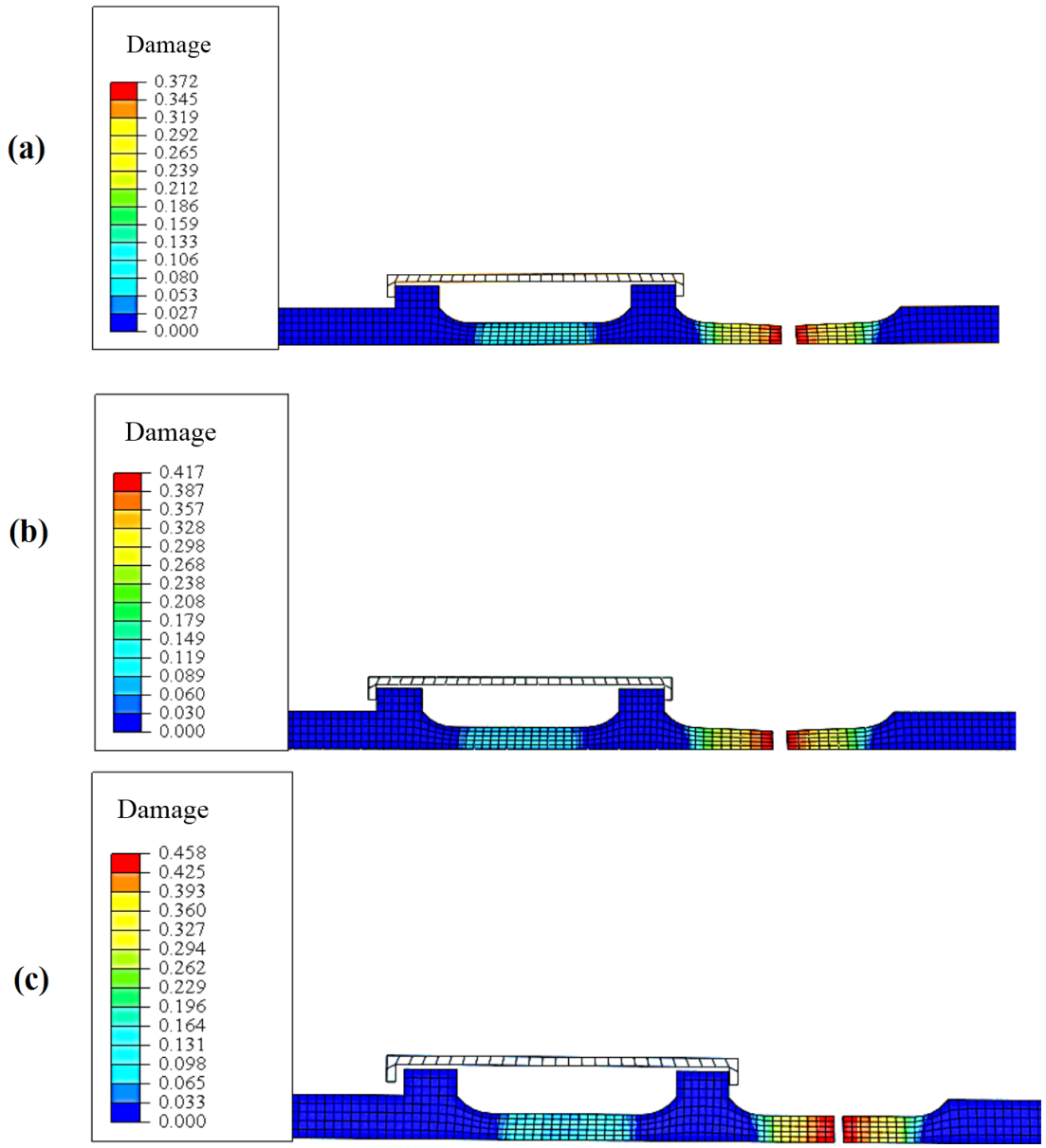

Fig. 18. Damage contours in the real segment of specimen at the strain rates of a) 630 s^{-1}, b) 1115 s^{-1}, and c) 1700 s^{-1}.

Table 7
Damage parameter for different strain rates and plastic strain.

Plastic strain (mm/mm)	Strain rate (1/s)					
	630		1115		1700	
	Experiment	VUSDFLD	Experiment	VUSDFLD	Experiment	VUSDFLD
0.061	0.067	0.061	0.090	0.083	0.105	0.920
0.121	0.125	0.142	0.182	0.170	0.212	0.195
0.168	0.194	0.180	0.218	0.197	0.274	0.248
0.229	0.215	0.221	0.254	0.262	0.297	0.284

6. Conclusions

In this paper, the Bonora damage model was modified by considering the effect of strain rate on material damage evolution. It was shown that two parameters of Bonora damage model, critical damage parameter, and damage exponent are dependent on strain rate. The dependency was defined by nonlinear relations. The two parameters were obtained from quasi-static and dynamic stress-strain curves using a curve fitting technique. In order to validate the modified model, it was implemented in ABAQUS/Explicit subroutines (VUSDFLD). A reasonable agreement was obtained between the experimental measurements and numerical predictions using the VUSDFLD subroutine. The numerical and experimental results showed that damage increased with strain rate.

References

[1] L.M. Kachanov, Introduction to Continuum Damage Mechanics, Springer Science & Business Media, Dordrecht, 10 (2013).

[2] A.L. Gurson, Continuum theory of ductile rupture by void nucleation and growth: Part I-Yield criteria and flow rules for porous ductile media, J. Eng. Mater. Technol., 99(1) (1977) 2-15.

[3] C.C. Chu, A. Needleman, Void nucleation effects in biaxially stretched sheets, J. Eng. Mater. Technol., 102(3) (1980) 249-256.

[4] G. Rousselier, Finite deformation constitutive relations including ductile fracture damage, Three-dimensional Constitutive Relations and Ductile Fracture, (1981) 318-343.

[5] G. Rousselier, Ductile fracture models and their potential in local approach of fracture, Nucl. Eng. Des., 105(1) (1987) 97-111.

[6] J. Lemaitre, A continuous damage mechanics model for ductile fracture, J. Eng. Mater. Technol., 107(1) (1985) 83-89.

[7] G.Z. Voyiadjis, P.I. Kattan, A plasticity-damage theory for large deformation of solids-I, Theoretical formulation, Int. J. Eng. Sci., 30(9) (1992) 1089-1108.

[8] N. Bonora, A nonlinear CDM model for ductile failure, Eng. Fract. Mech., 58(1-2) (1997) 11-28.

[9] L.M. Kachanov, Time of the rupture process under creep conditions, Izu. Akad. Nauk SSR Otd. Tech., 8 (1958) 26-31.

[10] L. Hao, P. Ke, W. June, An anisotropic damage criterion for deformation instability and its application to forming limit analysis of metal plates, Eng. Fract. Mech., 21(5) (1985) 1031-1054.

[11] J. Lemaitre, A Course on Damage Mechanics, Springer Science & Business Media, (2012).

[12] N. Bonora, G. Testa, A. Ruggiero, G. Iannitti, D. Gentile, Continuum damage mechanics modelling incorporating stress triaxiality effect on ductile damage initiation, Fatigue Fract. Eng. Mater. Struct., 43(8) (2020) 1755-1768.

[13] N. Bonora, G. Testa, A. Ruggiero, G. Iannitti, D. Gentile, Modification of the Bonora Damage Model for shear failure, Frattura ed Integrità Strutturale, 12(44) (2018) 140-150.

[14] C. Pei, W. Zeng, H. Yuan, A damage evolution model based on micro-structural characteristics for an additive manufactured superalloy under monotonic and cyclic loading conditions, Int. J. Fatigue, 131 (2020) 105279.

[15] Z. Guo, D. Huang, X. Yan, X. Zhang, M. Qi, J. Fan, A damage coupled elastic-plastic constitutive model and its application on low cycle fatigue life prediction of turbine blade, Int. J. Fatigue, 131 (2020) 105298.

[16] A. Yadollahi, N. Shamsaei, Y. Hammi, M.F. Horstemeyer, Quantification of tensile damage evolution in additive manufactured austenitic stainless steels, Mater. Sci. Eng. A, 657 (2016) 399-405.

[17] M. Kumar, P.M. Dixit, A nonlinear ductile damage growth law, Int. J. Damage Mech., 24(7) (2014) 1070-1085.

[18] S. Chandrakanth, P.C. Pandey, An isotropic damage model for ductile material, Eng. Fract. Mech., 50(4) (1995) 457-465.

[19] B.K. Thakkar, P.C. Pandey, A high-order isotropic continuum damage evolution model, Int. J. Damage Mech., 16(4) (2007) 403-426.

[20] A.J. Gillard, S.F. Golovashchenko, A.V. Mamutov, Effect of quasi-static prestrain on the formability of dual phase steels in electrohydraulic forming, J. Manuf. Process., 15(2) (2013) 201-218.

[21] A. Hassannejadasl, D.E. Green, S.F. Golovashchenko, F. Sergey, J. Samei, C. Maris, Numerical modelling of electrohydraulic free-forming and die-forming of DP590 steel, J. Manuf. Proc., 16(3) (2014) 391-404.

[22] M. Brünig, S. Gerke, J. Tix, Micro-mechanical numerical analyses on the effect of stress state on ductile damage under dynamic loading conditions, Lat. Am. J. Solids Struct., 15(8) (2018) e85.

[23] G.H. Majzoobi, K. Rahmani, A. Atrian, An experimental investigation into wear resistance of Mg-SiC nanocomposite produced at high rate of compaction, J. Stress Anal., 3(1) (2018) 35-45.

[24] G.H. Majzoobi, K. Rahmani, M. Kashfi, The effect of pre-compaction on properties of Mg/SiC nanocomposites compacted at high strain rates, J. Stress Anal., 4(2) (2020) 19-28.

[25] N. Bonora, D. Gentile, P.P. Milella, G. Newaz, F. Iacoviello, Ductile damage evolution under different strain rate conditions, Proceedings of the ASME 2000 International Mechanical Engineering Congress and Exposition. Crashworthiness, Occupant Protection and Biomechanics in Transportation Systems. Orlando, Florida, USA, 246 (2000) 145-153.

[26] I. Sari Sarraf, D.E. Green, A. Jenab, Damage evolution and void coalescence in finite-element modelling of DP600 using a modified Rousselier model, Eng. Fract. Mech., 196 (2018) 168-190.

[27] G.R. Johnson, W. Cook, A constitutive model and data for materials subjected to large strains, high strain rates, and high temperatures. In Proceedings of the 7th International Symposium on Ballistics, Hague, Netherlands, (1983).

[28] E. Voce, The relationship between stress and strain for homogeneous deformation, J. Inst. Met., 74 (1948) 537-562.

[29] Y. Cao, B. Karlsson, J. Ahlström, Temperature and strain rate effects on the mechanical behavior of dual phase steel, Mater. Sci. Eng. A, 636 (2015) 124-132.

[30] A.S. Khan, R. Liang, Behaviors of three BCC metal over a wide range of strain rates and temperatures: experiments and modeling, Int. J. Plast., 15(10) (1999) 1089-1109.

[31] C. Husson, S. Ahzi, L. Daridon, T. Courtine, Continuum damage modeling for ductile metals under high strain rate deformation, J. phys. IV (Proceedings), 110 (2003) 63-68.

[32] S.S. Jafari, G.H. Majzoobi, E. Khademi, M. Kashfi, Development of a new technique for measuring damage accumulation at high strain rates, Eng. Fract. Mech., 209 (2019) 162-172.

[33] G.H. Majzoobi, A.H. Mahmoudi, S. Moradi, Ductile to brittle failure transition of HSLA-100 Steel at high strain rates and subzero temperatures, Eng. Fract. Mech., 158 (2016) 179-193.

[34] G.R. Johnson, W.H. Cook, Fracture characteristics of three metals subjected to various strains, strain rates, temperatures and pressures, Eng. Fract. Mech., 21(1) (1985) 31-48.

[35] T. Holmquist, G. Johnson, Determination of constants and comparison of results for various constitutive models, J. phys., IV, EDP Sciences, 01 (C3) (1991) C3-853-C3-860.

[36] S. Walsh, D. Diamond, Non-linear curve fitting using microsoft excel solver, Talanta, 42(4) (1995) 561-572.

[37] N. Bonora, A. Ruggiero, D. Gentile, S. De Meo, Practical applicability and limitations of the elastic modulus degradation technique for damage measurements in ductile metals, Strain, 47(3) (2011) 241-254.